Research Square

Preprints are preliminary reports that have not undergone peer review.
They should not be considered conclusive, used to inform clinical practice,
or referenced by the media as validated information.

Stress distribution law of function gradient cement sheath with iron fillings and the discussion of casing deformation prevention in geothermal wells

Yan Yan

yansanbao302@163.com

CNPC Tubular Goods Research Institute

Yang Shangyu

CNPC Tubular Goods Research Institute

Zhao Xinwei

CNPC Tubular Goods Research Institute

Zhang Bin

China National Petroleum Corporation (China)

Song Lei

China National Petroleum Corporation (China)

Research Article

Keywords: Functional gradient cement sheath, Casing deformation, Hot dry rock, The compressive strength, Iron fillings

Posted Date: June 5th, 2026

DOI: https://doi.org/10.21203/rs.3.rs-8856565/v1

License: This work is licensed under a Creative Commons Attribution 4.0 International License.
Read Full License

Additional Declarations: Competing interest reported. We confirm that there are no potential competing interests for this article.

Stress distribution law of function gradient cement sheath with iron fillings and the discussion of casing deformation prevention in geothermal wells

Yan Yan[1,*] Yang Shangyu[1] Zhao Xinwei[1] Zhang Bin[2] Song Lei[3] Xu Qunchao[2]

1.State Key Laboratory of Oil and Gas Equipment, CNPC Tubular Goods Research Institute, Xi'an, 710077, China;

2.CNPC Liaohe Oilfield Branch, Exploration and Development Department, Panjin, 124010, China;

3.CNPC Jilin Oilfield Branch, Exploration and Development Department, Songyuan, 13800, China

Abstract: Casing deformation is an important cause of wellbore failure of geothermal well. By adding iron filings into cement and changing the distribution of iron filings along the radial direction of wellbore, a new cement sheath with gradient mechanical performance is prepared called as functional gradient cement sheath. In this paper, the mechanical model of functionally gradient cement was set up, and the mechanical parameters were obtained through tests. The analytical solutions of stress field and displacement field of cement sheath were obtained by elastic thick-walled cylinder theory, and then the effectiveness of functional gradient cement for casing deformation prevention was investigated. The results show that the compressive strength and elastic modulus of cement containing iron chips are both enhanced. Among the exponentially distributed, linear form, quadratic functional form and uniform form, the quadratic functional distribution for the elastic modulus of the functionally graded cement sheath effectively reduces the stress at the cement/formation interface and the radial displacement within the cement sheath, thereby reducing the risk of damage to the cementing interface. For geothermal wells, it is recommended to use large-sized iron filings and control the content within 10% to balance the requirements of cement sheath modification and integrity assurance.

Key words: Functional gradient cement sheath, Casing deformation, Hot dry rock, The compressive strength, Iron fillings

1 Introduction

Dry hot rock is a clean geothermal resource with great potential. Its depth is more than 2 km, its temperature is more than 150 °C without water. The heat energy contained in dry hot rock with the distance of 3-10 km from crust is equivalent to about 246 million tons of oil [1]. At present, developed countries such as the United States, France, Italy have used dry hot rock for power generation and heating [2]. There have been 46 projects of dry hot rock in the world up to 2023 [3]. A large number of dry hot rock has been found in China, such as Gonghe Basin in Qinghai Province, Maojingba-Qijia Town in Hebei Province, Longnan City in Jiangxi Province [4-5]. Due to the high temperature and high pressure of dry hot rock, the wellbore of geothermal well faces more severe problem such as casing deformation and sealing failure than that of conventional oil and gas wells [6-8].

The high temperature and high pressure of dry hot rock can easily cause the formation creep, which leads to the shrinkage of wellbore. Kinoshita et al [9] found that the creep failure time of granite at 80℃ was only 70% of that at 20℃. Yang et al [10] set up a three-dimensional finite element model of deep salt rock-cement-casing system to investigate the effects of formation dip, well inclination, formation thickness and mechanical parameters on casing equivalent stress and deformation under the non-uniform in-situ stress. Aiming at the theoretical research on wellbore failure caused by formation deformation, Yin et al [11-12] obtained the wellbore loading under in-situ stress by elastic theory and numerical method, and investigated the stress distribution of the cementing interface. Last et al [13] studied the casing displacement caused by tectonic stress. Li et al [14] used elastic theory and finite element method to study the stress distribution of inclined wellbore. Wu et al [15] investigated the influence of formation parameters, casing parameters, cement parameters on casing stress by using elastic mechanics, considering the influence of formation creep. For cement materials, Ma [16] added a little amount of micro-silica sand to effectively

Corresponding author：yanyan3@cnpc.com.cn

improve the strength of cement for thermal production wells. Giedrius et al [17] found that the mechanical properties of concrete could be improved by adding 5%-20% rubber particles in cement. Wille et al [18] measured the tensile strength of ultra-high performance cement added with steel fiber, and found that the increase of tensile strength was more obvious when micro steel fiber or torsion steel fiber was used. Delarrad [19] et al investigated the mechanical modification of cement based on the particle grading theory. Zhang [20] studied the strength and microstructure of cement by adding iron.

To sum up, the mechanical parameters of cement can be effectively improved by adding some improved materials[21-22] (fibers, barite, etc.), however, domestic and foreign scholars have treated cement as uniform materials for scientific research for cement sheath. Through the study of functional gradient material, it was found that the strength of the cement sheath can be effectively improved by adjusting the modified material to a certain distribution pattern[23] along the radial direction of the cement sheath. Based on the previous studies [24-25], iron filings, as an improved material, can effectively enhance the strength and toughness of cement-based materials. The cement sheath with gradual mechanical properties is prepared by changing the distribution of iron filings along the wellbore, which is called functional gradient cement sheath. After determining the mechanical parameters of the sample, the analytical solutions for the stress field and displacement field of the functional gradient cement sheath were obtained based on the elastic mechanics theory of thick-walled cylinders. These results were compared with the finite element calculation results to verify their accuracy. Finally, the influence law of the arrangement mode of iron filings on the stress field within the cement sheath was analyzed.

2 Functional gradient cement sheath mechanical model with iron filings

2.1 *Geometric model*

The axial deformation of the borehole is generally ignored due to the extended length along the axis, that is, the variation of axial strain is not considered, thus, the borehole of oil and gas well is simplified to the plane strain problem. According to the working condition of the wellbore, a mechanical model of functional gradient cement sheath with iron filings was set up without considering the influence of formation deviation stress field, as shown in **Fig.1**.

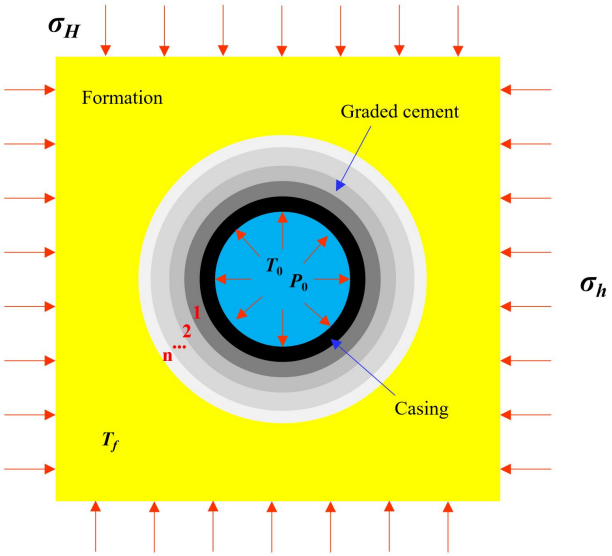


Fig.1 Mechanical model

In **Fig.1**, casing and formation are isotropous materials. The wellbore system is mainly subjected to in-situ stress, casing pressure P_0, casing temperature T_0 and formation temperature T_f. According to the previous research, the compressive strength of cement with the iron filings becomes lower when the iron filings content is below 15%.

But the distribution of iron filings in the cement is different, its mechanical properties and mechanical parameters are different. The cement with specific iron filings can be regarded as a new isostatic material. It is assumed that the functionally gradient cement is viewed as the superposition of layers by different materials, and the thickness of each layer is determined according to the distribution of iron filings in the radial direction.

The entire wellbore system consists of n+2 layers, where the layer 0 is casing, the layer n+1 is formation, and the layer from 1 to n is cement sheath. The elastic modulus of layer i is set as E_i, Poisson's ratio is set as μ_i, inner radius is set as R_i, and outer radius is set as R_{i+1}.

2.2 *Governing equation*

2.2.1 Thermo-solid coupling

There is difference between the fluid temperature in wellbore and the formation temperature. When the heat conduction of wellbore enters a steady state, its governing equation can be expressed as [24] :

$$\delta t_{1,ii} + h\left(t_1 - \bar{t}_1\right) = 0 \tag{1}$$

where δ is the conductivity coefficient; h is the convective heat transfer coefficient; t_1 is the temperature; $\bar{t}_1$ is the formation temperature.

The temperature boundary conditions are:

$$\begin{cases} t_1 = \bar{t}_1 & \text{on } \Gamma_{t_1} \\ \delta t_{1,\mathrm{n}} = \bar{Q}_1 & \text{on } \Gamma_{Q_1} \end{cases} \tag{2}$$

where Γ is the boundary of the thermal field; $\bar{Q}_1$ is the heat flow on the boundary.

Governing equation of wellbore structure field is:

$$\sigma_{ij,j} + f_i = 0 \tag{3}$$

where σ is stress; f is physical force.

The geometric equation is:

$$\varepsilon_{i,j} = \frac{1}{2}\left(u_{i,j} + u_{j,i}\right) \tag{4}$$

where ε is the strain and u is the displacement.

Thermosolid coupling constitutive relationship is:

$$\sigma_{i,j} = E^{ijkl}\left(\varepsilon_{kl} - \alpha_{kl}\Delta t_1\right) \tag{5}$$

where E is the elastic modulus; α is the expansion coefficient; $\triangle t_1$ is the variable temperature.

The boundary condition of structural field:

$$\begin{cases} u_{ij} = \bar{u}_j & \text{on } \Gamma_u \\ \sigma_{ij} n_j = \bar{f}_i & \text{on } \Gamma_f \end{cases} \tag{6}$$

where $\bar{u}_j$ is the displacement vector; $\bar{f}_i$ is the force vector; n_j is the surface component.

As can be seen from *Eq*(6), the stress is obtained from the linear superposition of structural stress and temperature stress, so the stress component in the thermosolid coupling field can be combined structural stress with temperature stress.

2.2.2 Structural field stress and displacement

Any layer of the material in the functional gradient cement model satisfies the thick-walled cylinder theory in elasticity, so the stress distribution of any layer under uniform pressure can be expressed as:

$$\begin{cases} \sigma_\rho = \dfrac{\dfrac{R^2}{\rho^2}-1}{\dfrac{R^2}{r^2}-1} q_1 - \dfrac{1-\dfrac{r^2}{\rho^2}}{1-\dfrac{R^2}{r^2}} q_2 \\ \sigma_\varphi = \dfrac{\dfrac{R^2}{\rho^2}+1}{\dfrac{R^2}{r^2}-1} q_1 - \dfrac{1+\dfrac{r^2}{\rho^2}}{1-\dfrac{r^2}{R^2}} q_2 \end{cases} \tag{7}$$

where q_1 is the inner pressure of the ring, q_2 is the outer pressure of the ring, R is the outer radius, r is the inner radius, ρ is the radius, $\sigma\rho$ is the radial stress and σφ is the circumferential stress.

The displacement expression of any layer combined with geometric equations and physical equations can be obtained as follows:

$$\begin{cases} u_\rho = \rho \cdot \varepsilon_\varphi = \rho \cdot \dfrac{1-\mu^2}{E}\left(\sigma_\varphi - \dfrac{\mu}{1-\mu}\sigma_\rho\right) \\ u_\varphi = 0 \end{cases} \tag{8}$$

where u_ρ is the radial displacement; u_φ is the circumferential displacement, and ε_φ is the circumferential strain.

Continuity equation is:

$$u_\rho^i \Big|_{\rho=R_{i+1}} = u_\rho^{i+1} \Big|_{\rho=R_{i+1}} \quad i = 0,1,2,\cdots,n \tag{9}$$

where u_ρ^i is the radial displacement of the layer *i*.

From *Eq*(9), equations can be constructed, shown as below:

$$\begin{bmatrix} K_{11} & K_{12} & 0 & 0 & \cdots & 0 & 0 & 0 \\ K_{21} & K_{22} & K_{23} & 0 & \cdots & 0 & 0 & 0 \\ 0 & K_{32} & K_{33} & K_{34} & \cdots & 0 & 0 & 0 \\ \vdots & \vdots & \vdots & \vdots & \ddots & \vdots & \vdots & \vdots \\ 0 & 0 & 0 & 0 & \cdots & K_{(n-1)(n-2)} & K_{(n-1)(n-2)} & K_{(n-1)n} \\ 0 & 0 & 0 & 0 & \cdots & 0 & K_{(n-1)n} & K_{nn} \end{bmatrix} \begin{Bmatrix} P_1 \\ P_2 \\ P_3 \\ \vdots \\ P_{n-1} \\ P_n \end{Bmatrix} = \begin{Bmatrix} -K_{10}P_0 \\ 0 \\ 0 \\ \vdots \\ 0 \\ -K_{n(n+1)}P_{n+1} \end{Bmatrix} \tag{10}$$

where

$$K_{n(n-1)} = \frac{1-\mu_{n-1}^2}{E_{n-1}} \frac{2R_{n-1}^2}{R_n^2 - R_{n-1}^2}$$

$$K_{nn} = \frac{1-\mu_{n-1}^2}{E_{n-1}}\left(-\frac{R_n^2 + R_{n-1}^2}{R_n^2 - R_{n-1}^2} + \frac{\mu_{n-1}}{1-\mu_{n-1}}\right) - \frac{1-\mu_n^2}{E_n}\left(\frac{R_{n+1}^2 + R_n^2}{R_{n+1}^2 - R_n^2} + \frac{\mu_n}{1-\mu_n}\right)$$

$$K_{n(n+1)}=\frac{1-\mu_n^2}{E_n}\frac{2R_{n+1}^2}{R_{n+1}^2-R_n^2}$$

Since P_0 and P_{n+1} are known conditions, P_1~P_n can be obtained by *Eq*(11).

2.2.3 Temperature stress and displacement

Thermal conductivity among casing, functional gradient cement sheath and formation can be expressed as [21]

$$\lambda=\lambda_0\left(1+bt\right) \tag{11}$$

From *Eq*(11), the thermal conductivity of layer i of the combined system is $\lambda_i=\lambda_{0i}\left(1+b_it\right)$, and then the linear heat flow rate q_i of layer i can be obtained:

$$q_i=\frac{2\pi\lambda_{mi}\left(T_{i-1}-T_i\right)}{\ln\dfrac{R_i}{R_{i-1}}},\ \lambda_{mi}=\lambda_{0i}\left(1+\frac{b_i}{2}\left(T_{i-1}+T_i\right)\right) \tag{12}$$

where λ_{mi} is the average thermal conductivity of the layer i, $T_{i\text{-}1}$ is the inner wall temperature of the layer i, T_i is the outer wall temperature of the layer i, $R_{i\text{-}1}$ is the inner radius of the layer i, R_i is the outer radius of the layer i.

The equation for solving the stable temperature field of the combined system can be expressed as:

$$q_i=q_{i+1} \tag{13}$$

From *Eq*(13), the temperature of interface T_i (i=1, 2, 3, ... , n-1) can be calculated by the trial method [22]. By substituting $\Delta T_{i-1}=T_{i-1}-T_f$, $\Delta T_i=T_i-T_f$ into *Eq*(12), the stable temperature field distribution of layer i can be obtained:

$$T_i\left(r\right)=\frac{1}{\ln\dfrac{R_i}{R_{i+1}}}\left(\Delta T_{i-1}\ln\frac{R_i}{r}-\Delta T_i\ln\frac{R_{i-1}}{r}\right) \tag{14}$$

The boundary conditions for solving the thermal stress of the combined system are:

$$\sigma_r^1\Big|_{r=R_0}=0\qquad\sigma_r^n\Big|_{r=R_n}=0 \tag{15}$$

By solving the displacement potential function satisfying the equilibrium differential equation, the stress component corresponding to the displacement is obtained. The stress supplementary solution σ_r=σ_φ=F, $\tau_{r\varphi}$=0 is obtained from the stress function $\phi=\frac{F}{2}r^2$, and the temperature stress of the layer i is finally obtained as follows:

$$\begin{cases}\sigma_r^i=\sigma_r^{'}+\sigma_r^{''}=-\dfrac{E_i\alpha_i}{r^2}\left[\int T_i\cdot rdr+H_i\right]+F_i\\ \sigma_\varphi^i=\sigma_\varphi^{'}+\sigma_\varphi^{''}=\dfrac{E_i\alpha_i}{r^2}\left[\int T_i\cdot rdr+H_i-T_i\cdot r^2\right]+F_i\\ \tau_{r\varphi}^i=\tau_{r\varphi}^{'}+\tau_{r\varphi}^{''}=0\end{cases} \tag{16}$$

where F_i and H_i are the constants of layer i related to mechanical parameters. Using geometric and physical equations in polar coordinates, the displacement of the layer i can be expressed as:

$$U_r^i = r\cdot\varepsilon_\varphi^i = \frac{\alpha_i}{r}(1+\mu_i)\left[\int_{R_{i-1}}^{r} T_i\cdot r dr + H_i\right] + \frac{r(1-\mu_i)F_i}{E_i} \tag{17}$$

In *Eq*(15) and (16), 2*n*+2 equations need to be established to solve the temperature stress. Using *Eq*(17) and the stress/displacement continuity conditions at the interface of each layer, equations are shown as *Eq*(18) :

$$\begin{bmatrix}
s_1^0 & 1 & 0 & 0 & \cdots & 0 & 0 & 0 & 0 & \cdots & 0 & 0 & 0 & 0 \\
s_1^1 & 1 & s_1^2 & -1 & \cdots & 0 & 0 & 0 & 0 & \cdots & 0 & 0 & 0 & 0 \\
s_1^3 & s_1^4 & s_1^5 & s_1^6 & \cdots & 0 & 0 & 0 & 0 & \cdots & 0 & 0 & 0 & 0 \\
\vdots & \vdots & \vdots & \vdots & \ddots & \vdots & \vdots & \vdots & \vdots & \ddots & \vdots & \vdots & \vdots & \vdots \\
0 & 0 & 0 & 0 & \cdots & s_i^1 & 1 & s_i^2 & -1 & \cdots & 0 & 0 & 0 & 0 \\
0 & 0 & 0 & 0 & \cdots & s_i^3 & s_i^4 & s_i^5 & s_i^6 & \cdots & 0 & 0 & 0 & 0 \\
\vdots & \vdots & \vdots & \vdots & \ddots & \vdots & \vdots & \vdots & \vdots & \ddots & \vdots & \vdots & \vdots & \vdots \\
0 & 0 & 0 & 0 & \cdots & 0 & 0 & 0 & 0 & \cdots & s_n^1 & 1 & s_n^2 & -1 \\
0 & 0 & 0 & 0 & \cdots & 0 & 0 & 0 & 0 & \cdots & s_n^3 & s_n^4 & s_n^5 & s_n^6 \\
0 & 0 & 0 & 0 & \cdots & 0 & 0 & 0 & 0 & \cdots & 0 & 0 & s_{n+1}^2 & 1
\end{bmatrix}
\begin{Bmatrix}
H_1 \\ F_1 \\ H_2 \\ \vdots \\ H_i \\ F_i \\ \vdots \\ F_n \\ H_{n+1} \\ F_{n+1}
\end{Bmatrix}
=
\begin{Bmatrix}
0 \\ m_1^1 \\ m_1^2 \\ \vdots \\ m_i^1 \\ m_i^2 \\ \vdots \\ m_n^1 \\ m_n^2 \\ m_{n+1}^1
\end{Bmatrix} \tag{18}$$

where $s_i^1 = -\frac{E_i\alpha_i}{R_i^2}$; $s_i^2 = -\frac{E_{i+1}\alpha_{i+1}}{R_i^2}$; $s_i^3 = \frac{\alpha_i}{R_i}(1+\mu_i)$; $s_i^4 = \frac{R_i(1-\mu_i)}{E_i}$; $s_i^5 = -\frac{\alpha_{i+1}}{R_i}(1+\mu_{i+1})$;

$s_i^6 = -\frac{R_i(1-\mu_{i+1})}{E_{i+1}}$; $m_i^1 = \frac{E_i\alpha_i}{R_i^2}\int_{R_{i-1}}^{R_i} T_i(r)\cdot r dr$; $m_i^2 = -\frac{\alpha_i}{R_i}(1+\mu_i)\int_{R_{i-1}}^{R_i} T_i(r)\cdot r dr$; $s_n^0 = -\frac{E_n\alpha_n}{R_n^2}$;

$m_n^1 = \frac{E_n\alpha_n}{R_n^2}\int_{R_{n-1}}^{R_n} T_n(r)\cdot r dr$

2.3 Model verification

To verify the calculation accuracy of the theoretical model, a finite element model under the same working conditions was set up. By comparing the calculation results of the theoretical model with those of the finite element analysis, the accuracy of the theoretical model was verified.

2.3.1 *Finite element geometric model*

To simplify the calculation, the following assumptions were made [26]: ① The rock and cement sheath are isotropic porous material; ② The influence of the stress field and temperature field is considered, and the influence of the seepage field is not considered. To eliminate the influence of the model size on the in-situ stress in the near wellbore area, the size of the formation was set to 5×5m (as shown in **Fig.2**), the outer diameter and wall thickness of the casing were 139.7mm and 10.54mm respectively, and the thickness of the cement sheath was 38.1mm. The densities of the casing, cement sheath, and formation rocks in the model were 7.85 g·cm^{-3}, 1.8 g·cm^{-3}, and 2.3 g·cm^{-3} respectively; the elastic modulus were 210 GPa, 9 GPa (there were differences in different distribution patterns at each position), and 25 GPa respectively; the Poisson's ratios were 0.27, 0.22, and 0.24 respectively.

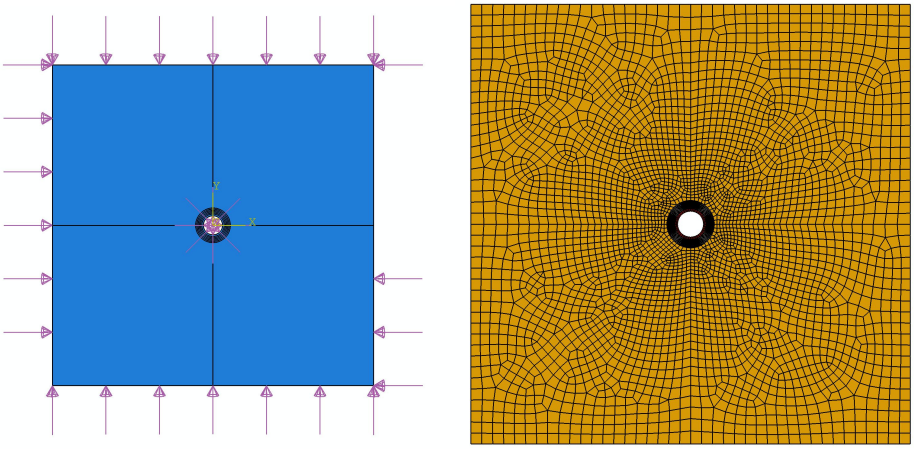


Fig.2 Geometric model

2.3.2 *Boundary conditions*

The pressure in the wellbore was set as 40 MPa, and the maximum/minimum horizontal in-situ stress of the formation is 36 MPa and 32 MPa respectively. Symmetrical constraints are set for the Z-direction of the formation boundary. The formation temperature is set at 90°C, and the initial temperature of the inner wall of the casing is 50°C. A rigid contact is set between the casing, cement sheath, and formation, and the friction coefficient of the contact surface is 0.2.

2.3.3 *Result comparison*

Fig.3 shows the radial stress distribution of the cement sheath and the formation when the iron filings inside the cement sheath are linearly distributed. It can be seen from **Fig.3** that the radial stress distribution of the cement sheath decreases radially from the inner to the outer. The theoretical calculation results of the linear and exponential distribution of iron filings inside the cement sheath are compared with the finite element calculation results (as shown in **Fig.4**), and it is found that the errors at different radial positions are all less than 10%, indicating that the accuracy of the model can meet the requirements of subsequent analysis.

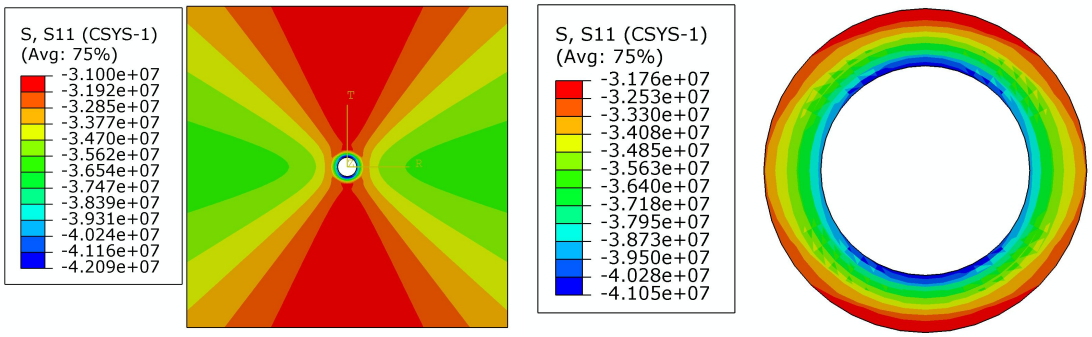


Fig.3 Finite element calculation results

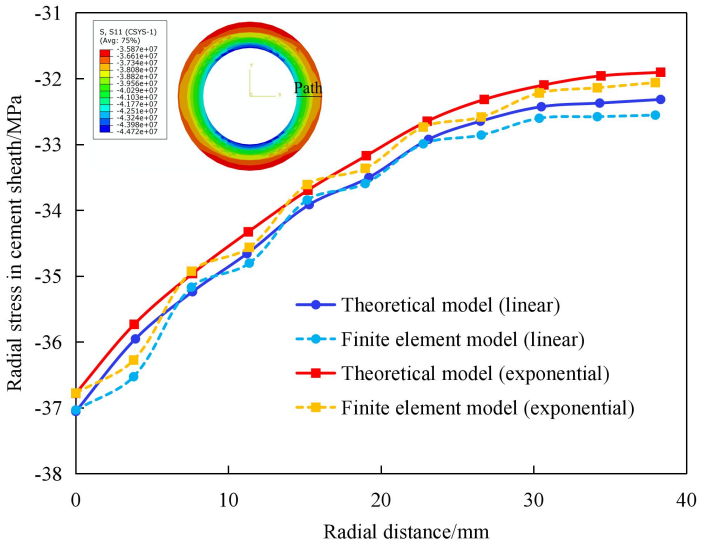


Fig.4 Comparison of theoretical model and finite element model

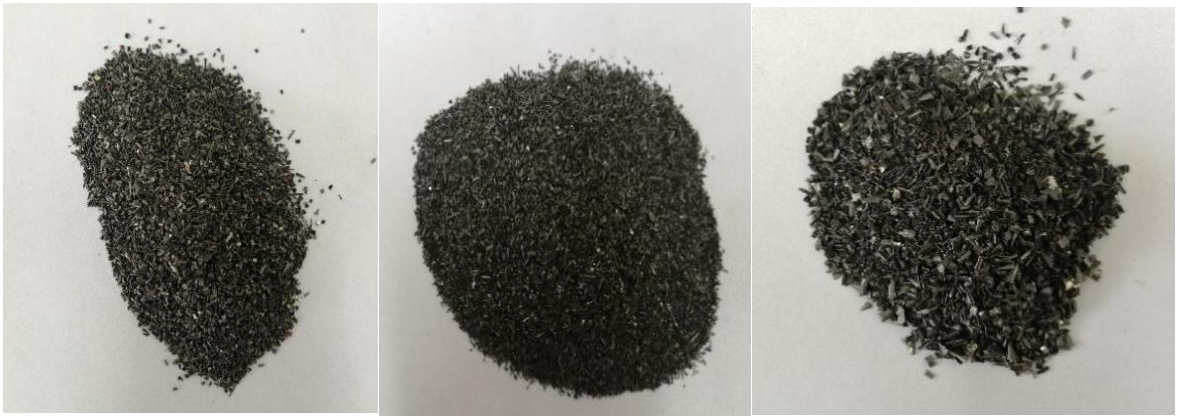
3 Experiment on mechanical parameters of cement containing iron filings

3.1 *Experimental materials and sample preparation*

Portland cement with grade P.O32.5 was used in the test, and its basic parameters[27] are shown in **Table 1**. Particle sizes of iron filings were screened as 0.5 mm, 1 mm and 2 mm, as shown in **Fig.5.** According to previous studies [28], 0.5 mm is generally regarded as a dividing point between fine particles and coarse particles; 1 mm is a commonly used representative of medium particle size; and 2 mm belongs to typical coarse particles. This selection can effectively reflect the nonlinear influence that variation in particle size (especially from sub-millimeter to millimeter scale) may have on the mechanical properties of cement materials. Therefore, iron filings with different particle sizes (0.5 mm, 1 mm and 2 mm) were added into cement slurry according to the mass ratio of iron/cement with 5%, 10% and 15% in this experiment. The cement was cured into the cube of 60mm×60mm×60mm, and the mass ratio of cement/water is 0.44. The water should be poured slowly, and the cement slurry should be be mixed evenly. In order to prevent the debris sinking due to gravity, cement slurry need to be stirred again, while avoiding the generation of bubbles in cement. The surface of cement should be smooth and there is no crack at the edges. Ejector was used to remove the mold after 24 hours to avoid collision, then the cement block was cured in the water for 28 days to complete the preparation of the sample.

Table 1 Basic properties of ordinary portl and cement（P.O 32.5）

Parameters	MgO/%	SO_3/%	Presetting time/min	Final setting time/min	Compressive strength with 7d/MPa	Specific surface area/(m^3/kg)
value	2.12	2.2	205	260	26.4	380



(a) Particle size 0.5mm (b) Particle size 1mm (c) Particle size 2mm

Fig.5 The iron filings

3.2 *Compression test*

The compressive strength was tested in accordance with GB/T 50081-2019. The experiment was repeated three times for each group to make the result accurate. The uniaxial compression process was shown in **Fig.6**, and the stress-strain curve of the measured sample was shown in **Fig.7**.



（a）Before compression （b）After compression

Fig.6 Compressive strength test

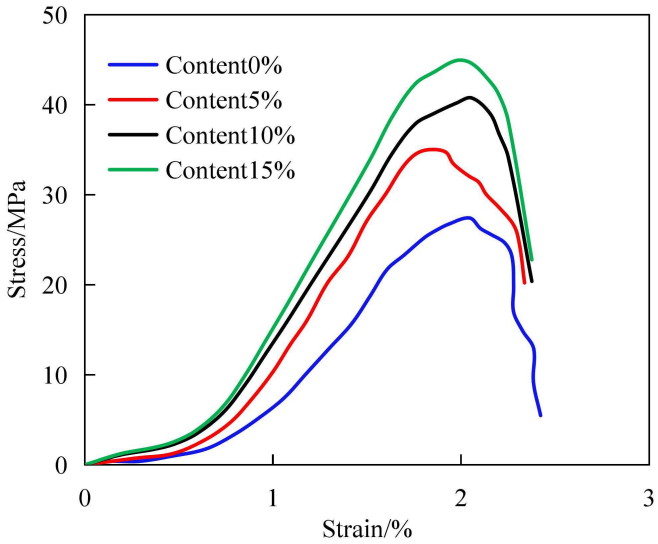


Fig.7 stress-strain curve

3.3 *Analysis of experimental results*

The compressive strength and elastic modulus of the sample were shown in **Table 2** with different particle size and amount of iron filings. As can be seen from **Table 2**, iron filings can effectively improve the compressive

strength and mechanical parameters of cement. With the increase of the iron amount, the compressive strength and elastic modulus of cement increase. **Fig.8** and **Fig.9** respectively illustrate the influence patterns of iron particle size and content on the compressive strength and elastic modulus of cement. It can be seen that the influence of iron content on the mechanical properties of cement is higher than that of particle size. That is, the variation in the amount of iron addition can effectively regulate the mechanical parameters of cement, thus providing a preparation scheme for the preparation of functional gradient cement sheath.

Table 2 Mechanical parameters of samples with different particle size and amount of iron filings

No	Iron size/mm	Iron content/%	Compressive strength/MPa	Average compressive strength/MPa	Elastic modulus/GPa	Average elastic modulus/GPa
1	0.5	5	34.6	34.2	11.8	10.8
2	0.5	5	34.1		10.5	
3	0.5	5	33.9		10.1	
4	0.5	10	41.5	41.7	12.6	13.3
5	0.5	10	40.9		13.7	
6	0.5	10	42.7		13.6	
7	0.5	15	43.3	43.3	14.4	14.1
8	0.5	15	43.5		13.7	
9	0.5	15	43.1		14.2	
10	1	5	37.6	37.1	11.1	11.3
11	1	5	36.8		11.4	
12	1	5	36.9		11.4	
13	1	10	42.2	42.6	13.4	13.6
14	1	10	42.8		13.8	
15	1	10	42.8		13.6	
16	1	15	45.5	45.5	15.4	15.7
17	1	15	45.5		15.9	
18	1	15	45.5		15.8	
19	2	5	34.1	34.6	10.9	11.7
20	2	5	35.4		11.6	
21	2	5	34.3		12.6	
22	2	10	44.5	44.5	14.4	13.9
23	2	10	44.5		13.8	
24	2	10	44.5		13.5	
25	2	15	48.1	47.5	16.2	16.2
26	2	15	47.7		16.3	
27	2	15	46.7		16.1	

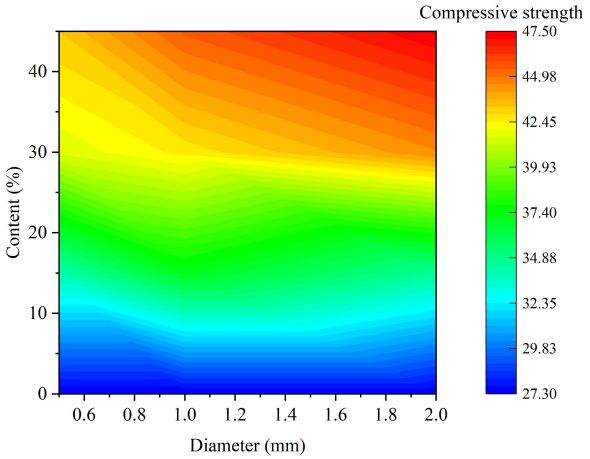


Fig.8 Cloud map of the influence of iron filings particle size and content on the compressive strength of cement

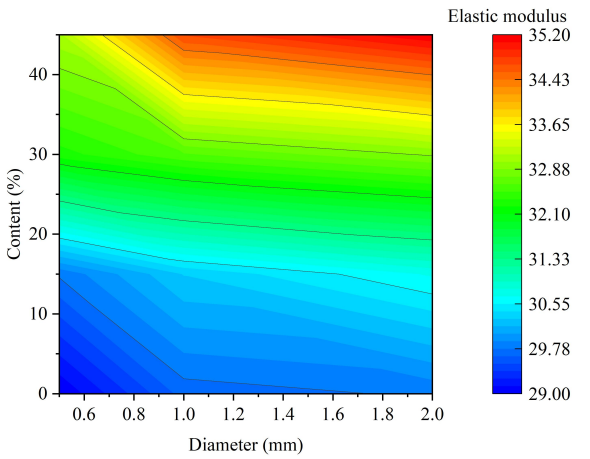


Fig.9 Cloud map of the influence of iron filings particle size and content on the elastic modulus of cement

4 Analysis of the influence law of functional gradient cement sheath containing iron filings

4.1 *Effect of iron distribution on stress and displacement field of functional gradient cement sheath*

The influence of iron distribution in the radial direction on the stress and displacement field of cement sheath was discussed in this section. According to the compressive test in section 3, the relationship between the iron content and the elastic modulus E can be determined. In the experiment, based on the combined process of layered pouring and directional vibration compaction [28], precisely control the content and particle size ratio of iron filings in each layer of the cement-based composite material, and using custom molds and vibration conditions to guide the directional arrangement of the iron filings, a continuous gradient variation in the content and size of iron filings from the surface to the interior of the sample was achieved. Therefore, the influence of the distribution pattern of elastic modulus along the radial direction on the stress/displacement field was investigated to determine the optimal distribution pattern of iron filings in the functional gradient cement sheath.

The total amount of iron filings was set as a fixed value, the distribution patterns of exponential form, linear form, quadratic parabola form and uniform distribution were selected in this paper, and its distribution function can be expressed as:

$$E=\begin{cases}9.5e^{3.1r}\\ 70r+3\\ 25\\ -1777.8r^{2}+1187.6r-163.28\end{cases} \tag{19}$$

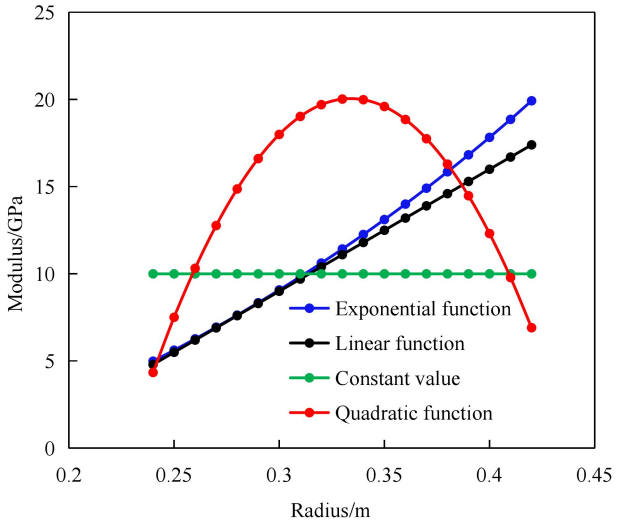


Fig.10 The elastic modulus variation under different functional form

The elastic modulus distribution along the radial direction is shown in **Fig.10**. The effects of modulus on stress/displacement field were investigated. **Fig.11** shows the radial stress distribution of the functional gradient cement sheath along the radial direction, **Fig.12** shows the circumferential stress distribution along the radial direction.

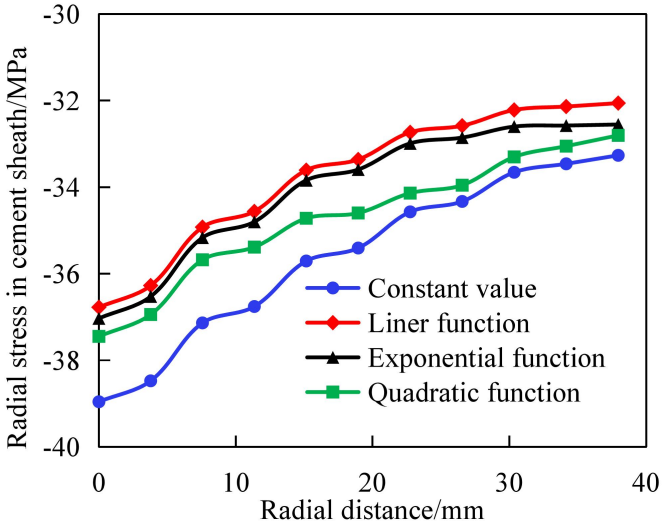


Fig.11 Radial stress curve of functional gradient cement sheath

It can be seen from **Fig.11** that the radial stress shows a decreasing trend from the center to the periphery along the radial direction regardless of how the iron filings are distributed within the cement sheath. When the iron filings are uniformly distributed at a fixed value, the radial stress is the highest; when they are distributed linearly, the radial stress is the lowest. Compared with the uniform distribution form, the radial stress in the linear distribution and exponential distribution forms is reduced by 2.1 MPa, 1.6 MPa, and 0.9 MPa respectively on average. From the perspective of radial stress, the linear distribution form of iron filings is the most optimal.

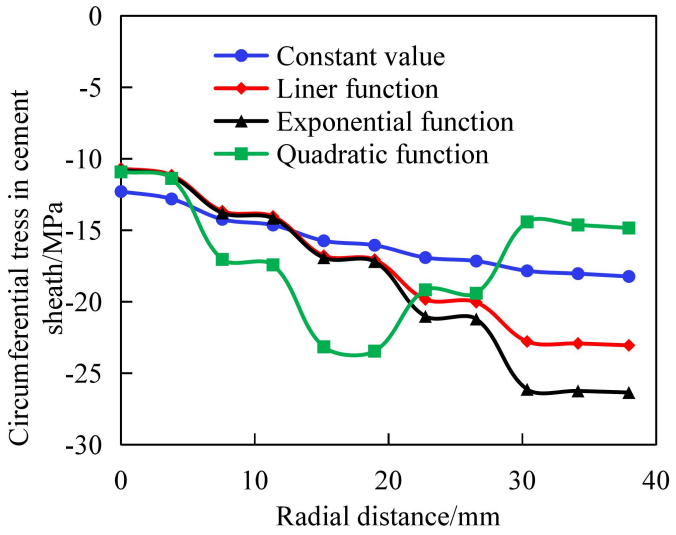


Fig.12 Hoop stress curve of functional gradient cement sheath

It can be seen from **Fig.12** that the circumferential stress near the interface in the linear distribution and the exponential distribution significantly increases compared with the uniform distribution, while the circumferential stress in the quadratic distribution shows a trend of increasing first and then decreasing. That is, the maximum circumferential stress in the quadratic distribution is located in the middle of the cement sheath. Compared with the uniform distribution, the circumferential stress increase at the cement/formation interface in the linear form and the exponential distribution is 27.2% and 42.9% respectively, while the radial stress in the quadratic form at the cement/formation interface decreases by approximately 19.6%. In the quadratic form, the circumferential stress at the bonding surfaces is less than that in the uniform distribution form. Therefore, the quadratic distribution can effectively reduce the failure probability of bonding surface. From the perspective of circumferential stress, the iron filings distribution in the quadratic distribution is the most optimal.

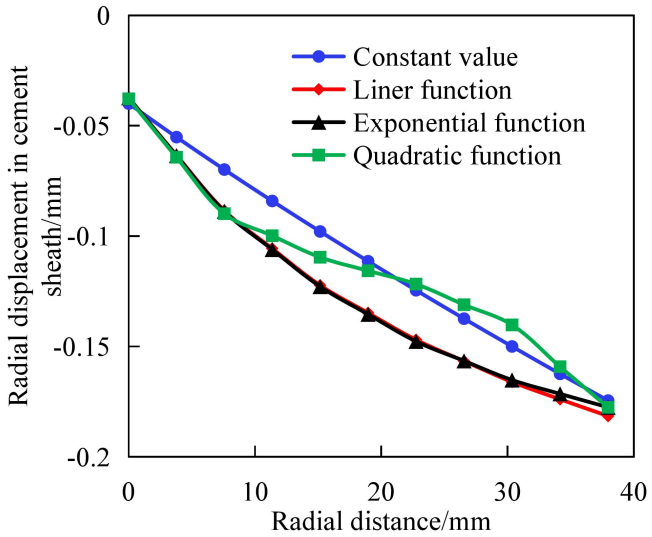


Fig.13 Radial displacement curve of functional gradient cement sheath

Fig.13 shows the radial displacement distribution along the radial direction. It can be seen from **Fig.13** that the radial displacement in the cement sheath increases with linear distribution or exponential distribution under the same loading. The radial displacement in the form of quadratic parabola firstly increases and then decreases. Inside the functionally graded cement sheath, the smaller the radial displacement, the lower the displacement transmitted to the casing. Therefore, it can effectively reduce the risk of the cementing interface damage and casing

deformation, thereby improving the reliability of the wellbore. In summary, the mechanical properties are optimal when the elastic modulus distributed in the form of quadratic parabola.

4.2 *Effect of iron size on stress field and displacement field of functionally graded cement sheath*

The effects of the stress and displacement on the inner wall of the cement with iron filings of 5%, 10% and 15% were investigated (The iron filings are linearly distributed) under the same boundary. **Fig.14** and **Fig.15** show the radial stress and circumferential stress distribution of the cement sheath along the radial direction with different particle sizes of iron filings. It can be seen from **Fig.14-Fig.15** that the variation patterns of radial stress and circumferential stress along the radial direction are basically the same under different iron contents. The larger the amount of iron filings, the lower the influence of iron filings size on radial stress and circumferential stress. The increase in circumferential stress will increase the risk of shear failure of the cement sheath. Therefore, it is advisable to use large-sized iron filings and keep the iron content within 10%.

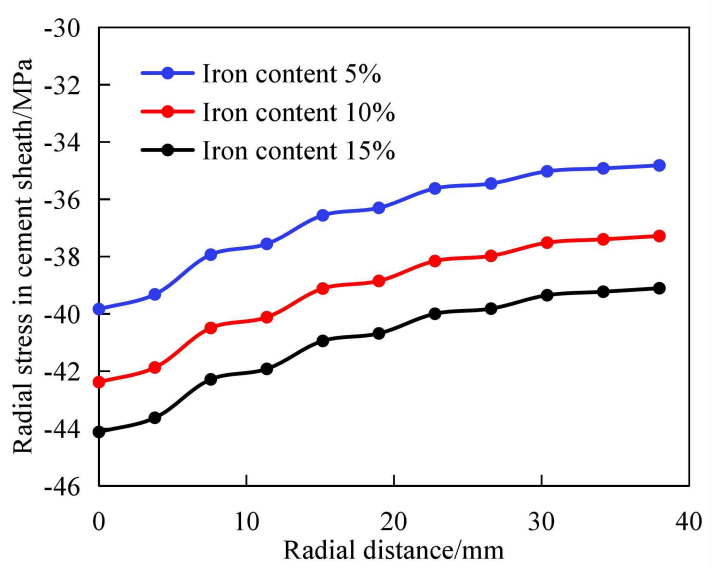


Fig.14 The radial stress of functional gradient cement sheath inner wall under different iron filings size

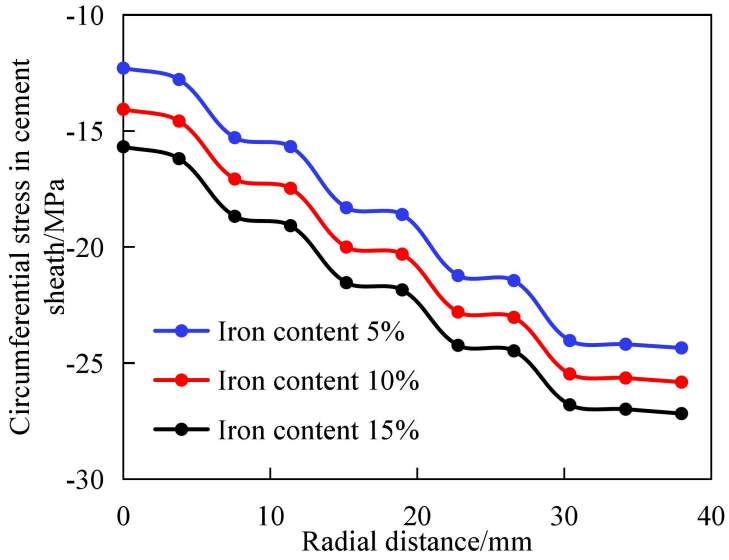


Fig.15 The hoop stress of functional gradient cement sheath inner wall under different iron filings size

5 The influence of iron filings parameters on the casing deformation

Fig.16 is a cloud chart illustrating the influence patterns of iron content and particle size on the deformation of

the casing. The radial displacement of the casing is jointly affected by the iron content and particle size, showing a distinct nonlinear change pattern. The color gradient in **Fig.16** indicates that the casing deformation increases with the increase in iron particle content and particle size, but the influence of particle size is much less than that of content. The reason is the addition of iron particles effectively enhances the compressive strength and elastic modulus of the cement matrix. A higher elastic modulus means that the overall stiffness of the cement is greater. When subjected to the same formation loading, internal pressure, and thermal stress, it can more effectively inhibit its own deformation and transfer smaller displacements to the internal casing through the cement bond surface, thereby significantly reducing the radial displacement of the casing.

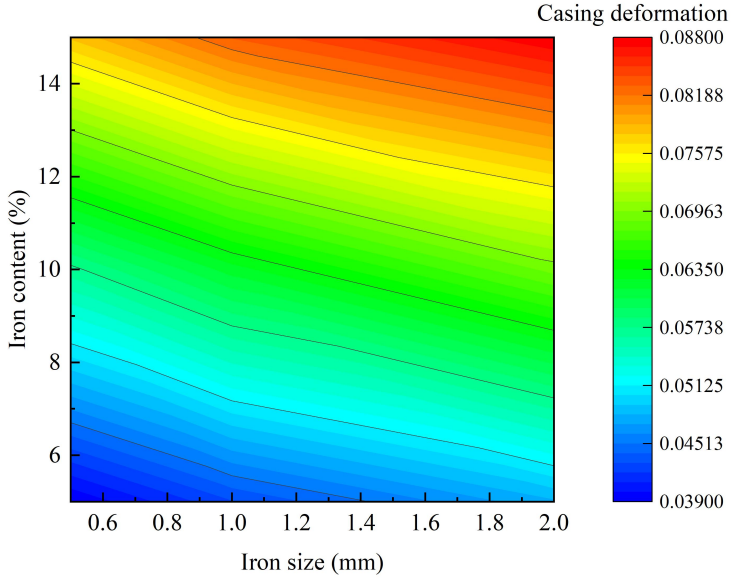


Fig.16 The influence law of iron filings content and particle size on the casing deformation

6 Conclusion

(1) The theoretical model of functional gradient cement sheath was set up, and the analytical solutions of stress field and displacement field were obtained. The iron filings can effectively increase the compressive strength and elastic modulus of cement.

(2) By analyzing the influence of iron distribution along the radial direction on the displacement and stress field of the functional gradient cement sheath, the quadratic distribution pattern can effectively reduce the stress at the cementing interface and radial displacement inside the cement sheath, thus reducing the risk of sealing failure.

(3) The particle size and the amount of iron filings have a great influence on the stress field and displacement field of cement sheath. As the iron content increases, the radial stress and circumferential stress of the cement sheath will significantly increase. To meet the requirements of cement modification and integrity protection, it is advisable to use large iron filings and control the iron content within 10%.

Funding

The authors would like to gratefully acknowledge the supports of Youth Project funded by Deep Earth Probe and Mineral Resources Exploration- National Science and Technology Major Project (2024ZD1000401), China National Petroleum Corporation Youth Science and Technology Special Project (2024DQ03030).

Declarations

The authors declared that they have no conflicts of interest in this work.

References

[1] Jello J, Baser T. Utilization of existing hydrocarbon wells for geothermal system development: A review. Applied Energy, 2023, 348: 121456.

[2] Wang PT, Wang SM, Wang GY, et al. Exploitation technology and productivity analysis of hydrothermal geothermal multi-branch wells. Geothermics, 2024, 117: 102883.

[3] Sun YX, Zhang X, Liu YS, et al. Prediction and optimization of productivity and lifespan in multi-well enhanced geothermal system. Applied Thermal Engineering, 2023, 234: 121155.

[4] Arbad N, Emadi H, Watson M. A comprehensive review of geothermal cementing from well integrity perspective. Journal of Petroleum Science and Engineering, 2022, 217: 110869.

[5] Yang Y, Li B, Che LL. Study on the performance and mechanism of high thermal conductivity and low-density cementing composite for deep geothermal wells. Energy, 2023, 285: 129429.

[6] Allahvirdizadeh, P., 2020. A review on geothermal wells: well integrity issues. Journal of Cleaner Production, 275, 124009.

[7] Cheng Guodong, Pang Xueyu, Sun Jinsheng, et al. Combined use of fly ash and silica to prevent the long-term strength retrogression of oil well cement set and cured at HPHT conditions. Petroleum Science, 2024, 21(2): 1122-1134.

[8] Deng Kuanhai, Zhou Niaotao, Lin Yuanhua, et al. Failure mechanism and control method of cement sheath sealing integrity under alternating thermal-stress coupling in geothermal wells. Renewable Energy, 2024, 226: 120448.

[9] Kinoshita N, Inada Y. Effects of high temperature on strength, deformation, thermal properties and creep of rocks. Journal of the Society of Materials Science, 2006, 55(5): 489–494.

[10] Yang S Y, Zeng B, Yan Y, et al. Research on casing deformation mechanism and prevention technology in salt rock creep formation. Journal of Petroleum Science and Engineering. 2023, 220: 111176.

[11] Yin YQ, Chen CW, Li PE. Theoretical solution of stress distribution in casing, cement ring and formation. Theoretical and Applied Mechanics, 2006, 38(6): 835-842.

[12] Liu K, Gao D L, Wang Y B., et al. Effect of local loads on shale gas well integrity during hydraulic fracturing process. Journal of Natural Gas Science and Engineering, 2017, 37(1): 291-302.

[13] Last N C, Mujica M, Pattillo P D, et al. Evaluation, impact, and management of casing deformation caused by tectonic forces in Andean Foothills, Colombia. SPE Drilling & Completion, 2006, 21(2): 116-124.

[14] Zhao C J, Li J, Liu G H, et al. Analysis of the influence of cement sheath failure on sustained casing pressure in shale gas wells[J]. Journal of Natural Gas Science and Engineering, 2019, 66(6): 244-254.

[15] Wu F, Chen J, Zou QL. A nonlinear creep damage model for salt rock. International Journal of Damage Mechanics 2019, 28(5): 758–71.

[16] Ma Z L, Hao H Y, Xie Z T, et al. Study on the effect of microsilica sand content on cementing strength of thermal recovery wells . Contemporary Chemical Research,2019, 000(009):72-74. .

[17] Giedrius G, Dzigita N. Crushed rubber waste impact of concrete basic properties. Construction and Building Materials, 2017, 140: 36-42.

[18] Wille K, Kim D J, Naaman A E. Strain-hardening UHP-FRC with low fiber contents. Smart Materials and structures, 2011, 44(3): 583-598.

[19] DeLarrad F, Sedran T. Optimization of ultra-high-performance concrete by the use of a packing model. Cement and Concrete Research, 1994, 24(6): 997-1009.

[20] Zhang G X. Effect of iron powder on strength and microstructure of cement mortar. Traffic Engineering and Technology for National Defence, 2021, 19(3):27-31.

[21] Malcom A. Grant, Paul F. Bixley, Ian G. Donaldson. Internal flows in geothermal wells: Their identification and effect on the wellbore temperature and pressure profiles. SPE Journal, 1983, 23(1): 168-176.

[22] Pedram Eskandari Sabzi, Alimorad Rashidi, Soheila Sharafinia. Lightweight cement composites incorporating novel graphene -alumina nanohybrid for unconventional geothermal and oil wells. Construction and Building Materials,

2025, 501: 144265.

[23] Cui Kaixiao, Jiang Guancheng, Yang Lili, et al. Preparation and properties of magnesium oxysulfate cement and its application as lost circulation materials. Petroleum Science, 2021, 18(5): 1492-1506.

[24] Tan Huijing, He Wei, Ye You, et al. Influence of polyvinyl alcohol coated porous Al_2O_3 ceramic waste particles on cement properties in geothermal applications. Construction and Building Materials, 2023, 376: 131046.

[25] Khizar Abid, Kayode Sanni, Catalin Teodoriu. Long-term experimental study of thermal conductivity and machine learning analysis of various cement mixtures for geothermal wells. Renewable Energy, 2025, 245: 122762.

[26] Yin Yue, Zhang Liwei, Mei Kaiyuan, et al. Experimental investigation on H2S-induced oilwell cement degradation under high-temperature conditions for geothermal applications. Geothermics, 2024, 121: 103023.

[27] Yan Yan, Cai Meng, Ma Wenhai, et al. Research on casing deformation prevention technology based on cementing slurry system optimization. Petroleum Science, 2024, 21(2): 1231-1240.

[28] Yang Yu, Li Bo Li, Che Lulu, et al. Study on the performance and mechanism of high thermal conductivity and low-density cementing composite for deep geothermal wells. Energy, 2023, 285: 129429.